Hybrid Monoliths for Magnetically-Driven Protein Separations

Telma Barroso, Teresa Casimiro, Ana M. Ferraria, Fábio Mattioli, Ana Aguiar-Ricardo, and Ana C. A. Roque**

Monoliths represent powerful platforms for isolation of large molecules with high added value. This work presents a hybrid approach for antibody (Ab) capture and release. Using mostly natural polymers and clean processes, it is possible to create macroporous monoliths with well-defined porous networks, tuneable mechanical properties, and easy functionalization with a biomimetic ligand specific for Ab. Magnetic nanoparticles (MNPs) are embedded on the monolith network to confer a controlled magnetic response that facilitates and accelerates Ab recovery in the elution step. The hybrid monolithic systems prepared with agarose or chitosan/poly(vinyl alcohol) (PVA) blends exhibit promising binding capacities of Abs directly from cell-culture extracts (120 ± 10 mg Ab g^{-1} support) and controlled Ab magnetically-assisted elution yielding $95 \pm 2\%$ recovery. Moreover, a selective capture of mAbs directly from cell culture extracts is achieved yielding a final mAb preparation with 96% of purity.

1. Introduction

Over the last decade, the global antibody (Ab) market has grown exponentially due to the increasing applications in research, pharmacology, diagnostics and therapy.[1] As an answer to such demand, new Ab purification approaches have been developed in order to obtain Ab with a high purity as imposed by regulatory agencies.[2,3] Typical Ab purification protocols rely on affinity chromatography,[1,4] but new polymeric affinity matrices have been proposed as an attempt to overcome limitations of traditional packed bed columns and membranes including: high pressure drop and high cost, low flow rates, weak mechanical properties and tendency for fouling.[5] Monoliths, cryogels and hydrogels form 3D porous structures with well interconnected large pores, which enable high fluxes and require small volumes and less time for efficient purification processes.[6–8] Several synthetic polymers have been used to develop such matrices.[9] However, regulatory laws are pressing the industry to redesign products and processes toward sustainable alternatives.[10] Chitosan (CHT),[11,12] agarose (AG)[13,14] and dextran (DXT)[15] are natural polymers used for biomedical and biotechnological purposes,[16,17] namely in the design of macroporous structures for cell growth,[18] isolation and immobilization of proteins,[19] drug delivery and tissue engineering.[20] Natural polymers present outstanding properties; they possess high density of functional chemical groups, fouling resistance, biocompatibility and biodegradability.[10] "Smart" or "intelligent" materials[21] are also interesting due to their capacity to respond to very slight changes (pH, temperature, light and electric or magnetic field) in the surrounding environment leading to modifications in shape, surface characteristics, solubility and others.[22,23] With the rapid development of nanotechnology, iron oxide magnetic nanoparticles (MNPs) are one of the most explored smart material in a wide range of applications including magnetic resonance imaging,[24,25] drug delivery,[26,27] immobilization of biomolecules and bioseparations.[28,29] In particular, MNPs can be combined with various polymers and functionalized with ligands commonly employed in chromatographic methods, leading to nano and micro absorbents suitable for Ab purification.[17,30–32] The combination of hydrogels or cryogels with MNPs has also been leading to different magnetic macroporous structures with interconnected pores in the micrometer range.[32–34] Additionally, these composite materials, in the presence of a moderate magnetic field, are able to deform which enable the flux of water or other fluids enhancing the release of biological agents as cells and proteins. This feature permit controlled actions and consequently faster processes but has never been explored for chromatographic applications.

Inspired by these features, this work aimed at 1) the design of hybrid monoliths following green chemistry guidelines, and

T. Barroso, T. Casimiro, Prof. A. Aguiar-Ricardo, Prof. A. C. A. Roque
REQUIMTE, Departamento de Química
Faculdade de Ciências e Tecnologia
Universidade Nova de Lisboa
2829–516 Caparica, Portugal
E-mail: air@fct.unl.pt; cecilia.roque@fct.unl.pt
A. M. Ferraria
CQFM and IN
Instituto Superior Técnico
Universidade de Lisboa
1049–001, Lisboa, Portugal
F. Mattioli
Center for Micro-BioRobotics@SSSA
Istituto Italiano di Tecnologia
Viale Rinaldo Piaggio 34, 56025, Pontedera, Italy

DOI: 10.1002/adfm.201400022

2) the evaluation of the hybrid monoliths as purification devices using a novel magnetically-assisted elution protocol. The hybrid concept results from the synergy between the capturing of Ab through affinity interactions and a magnetic response for improved Ab elution. Macroporous monoliths based on chitosan, agarose, dextran and PVA, with and without MNPs embedded, were prepared by combining freezing and lyophilization processes.[35] Conversely to the traditional procedures,[31,36,37] in this work the natural polymers were not chemically modified but physically entrapped by the polymeric network built from glycidyl methacrylate (GMA), acrylamide and bisacrylamide, that worked as monomers and crosslinking agents, respectively. This strategy assures the biodegradability of the monoliths, since the natural polymers remain unchanged, and offer a sustainable solution for robust materials processing. The macroporous materials were then aminated using plasma technology,[38,39] a solvent free technique, for further ligand coupling. The amination based on plasma treatment takes advantage of the high reactivity of argon(Ar)-plasma which generates free radicals sites located at monoliths surface, promoting in situ heterogeneous chemical reactions with gas-phase molecules like amines (1,6-hexanediamine, in this case). The functionalities introduced allowed the coupling of TPN-BM, a synthetic affinity ligand previously developed as a Protein A mimic.[40] The presence of MNPs at the monolithic porous network will confer a magnetic response to the material which facilitates Ab recovery by controlled shrinking.

This strategy intends to develop a smart, efficient, fast and eco-friendly approach for Ab purification which can be extended to other biotechnological and biomedical applications.

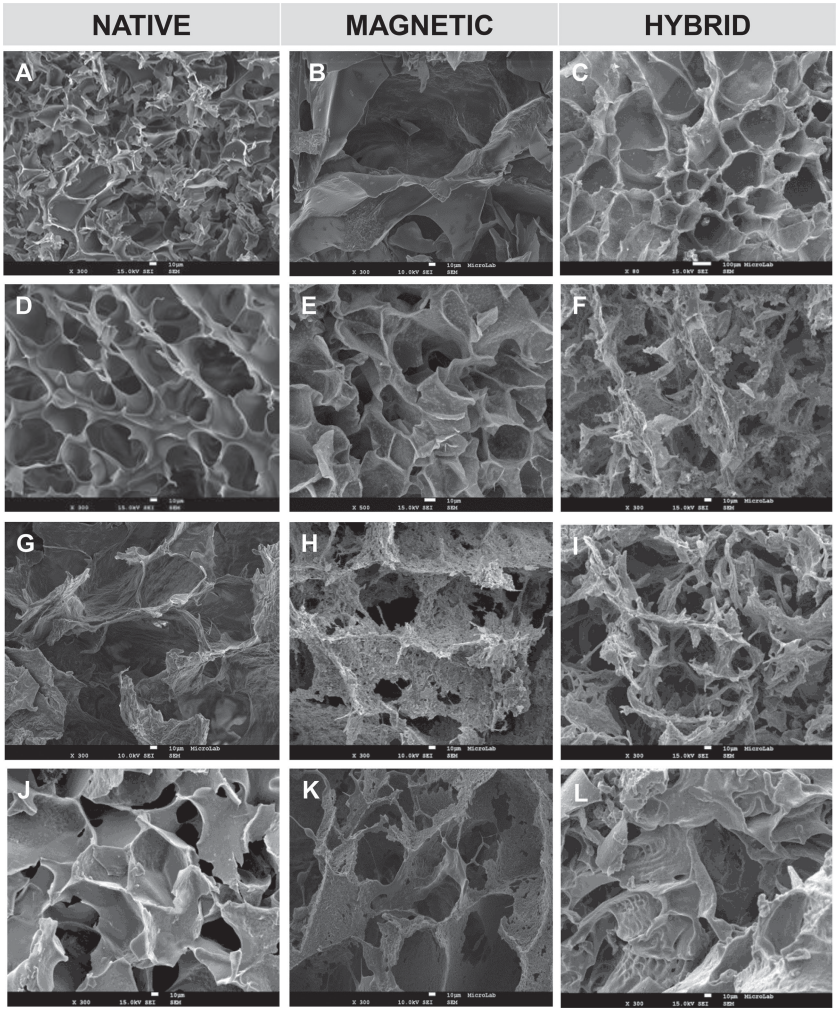

Figure 1. SEM images of natural-based monoliths before (native, N) and after MNP's incorporation (magnetic, M) and hybrid monoliths (magnetic with ligand TPN-BM coupled, M_TPN-BM): A) native chitosan monolith (CHT_N), B) magnetic chitosan monolith (CHT_M), C) hybrid chitosan monolith (CHT_M_TPB-BM), D) native chitosan blended with poly(vinyl alcohol) monolith (CP_N), E) magnetic chitosan blended with poly(vinyl alcohol) monolith (CP_M), F) hybrid chitosan blended with poly(vinyl alcohol) monolith (CP_M_TPN-BM), G) native agarose-based monolith (AG_N), H) magnetic agarose-based monolith (AG_M), I) hybrid agarose-based monolith (AG_M_TPN-BM), J) native dextran-based monolith (DXT_N), K) magnetic dextran-based monolith (DXT_M), and L) hybrid dextran-based monolith (DXT_M_TPN-BM). All the micrographs have a magnification of 300 and the scale bar in white indicates 10 μm.

2. Results and Discussion

2.1. Characterization of Native and Magnetic Monoliths

All monoliths, native (N-without MNPs) and magnetic (M-with MNPs), were characterized according to their morphological, mechanical, magnetic and physico-chemical properties and stability. **Figure 1** exhibits the SEM images of native (Figure 1A,C,E,G) and magnetic (Figure 1B,D,F,H) monoliths based on natural polymers. Regarding the porous network of both native and magnetic monoliths, it is noticeable that the addition of MNPs to the 3D structure did not influence significantly their architecture. The presence of well dispersed MNPs in the monoliths pore wall is evident. Moreover, depending on polymer composition, monolithic porous network can be adjusted and different designs can be achieved. Monoliths composed of chitosan (CHT; Figure 1A-B) crosslinked with *N,N'*-methylenebisacrylamide (MBA) and chitosan blended with poly(vinyl alcohol) and entrapped also by the crosslinked (MBA) network (CP; Figure 1D-E) exhibit smaller, spherical and heterogeneous pores. On the other hand, monoliths prepared from casting solutions of agarose (AG; Figure 1G,H) or dextran (DXT; Figure 1J,K) both, blended with glycidyl methacrylate (GMA) cryopolymerized with acrylamide, present a lacy structure with elongated pores. These supermacroporous structures were expected since monoliths based on agarose and dextran are known to form spongy

Table 1. Morphological and mechanical characterization of natural-based monoliths before (native (N)) and after magnetic nanoparticles embedding (magnetic (M)). All data was obtained from duplicated and triplicated measurements.

		CHT_N	CHT_M	CP_N	CP_M	AG_N	AG_M	DXT_N	DXT_M
Average pore size diameter [µm][a)]		17 ± 5	89 ± 5	53 ± 5	88 ± 5	73 ± 5	71 ± 5	96 ± 5	75 ± 5
Porosity [%][a)]		91 ± 2	90 ± 2	88 ± 2	86 ± 2	93 ± 2	92 ± 2	82 ± 2	98 ± 2
Water Flux [L m^{-2} h^{-1}]		142 ± 5	110 ± 7	294 ± 7	120 ± 9	102 ± 9	212 ± 9	100 ± 5	176 ± 8
Surface Area [m^2g^{-1}][a)]		2.7 ± 0.3	0.5 ± 0.2	0.4 ± 0.2	1.0 ± 0.2	1.0 ± 0.3	2.1 ± 0.3	3.0 ± 0.5	3.0 ± 0.5
Compressive Modulus [kPa]	Dry	2.3 ± 0.7	2.2 ± 0.5	0.6 ± 0.2	1.8 ± 12	0.7 ± 0.2	0.5 ± 0.1	5.3 ± 0.5	4.1 ± 0.4
	Wet	1.9 ± 0.3	0.4 ± 0.1	0.4 ± 0.2	0.5 ± 0.2	0.5 ± 0.2	0.3 ± 0.1	0.7 ± 0.2	0.5 ± 0.2

[a)]Determined for dried monoliths by mercury porosimetry analysis.

networks, independently of their processing method.[14,37,41] All monoliths presented as semi-rigid single blocks with dimensions of the mould where they were prepared. Still, monoliths were able to fit in any support which presents the same dimensions or even with a higher diameter, since all of them were able to swell and fit into various supports. The average pore size diameters and the porosity values calculated by MIP (mercury intrusion porosimetry) for each monolith before and after MNPs addition (**Table 1**) are in agreement with the SEM images. The magnetic monoliths exhibited some differences regarding the values of average pore size diameter comparing with the native ones. CHT and CP monoliths suffered a notorious enlargement from 17 and 53 to 89 and 88 µm respectively, after MNPs embedding, while monoliths prepared with agarose and dextran maintained average pore size diameters between 70 and 90 µm. In addition, porosity values are similar for all monoliths (82–91%). High porosity values were expected due to the freeze-drying method employed in monoliths production, which normally generates high porosities.[42,43] The specific surface area values obtained for all monoliths were within the range 0.5 and 3.0 m^2 g^{-1}, which is in agreement with obtained values of porosity, since the surface area varies inversely to the porosity.[44]

Materials for bioprocessing must be hydrophilic with well-organized porous networks to allow fast fluxes and easy permeations, and present mechanical stability to preserve their architecture. Table 1 also comprises the estimated water fluxes and compressive modulus measured, which translate the hydrophilicity and stiffness of the material respectively, for all polymeric monoliths before and after MNPs addition. All monoliths presented values of water fluxes between 100 and 300 L m^{-2} h^{-1}. CHT and CP monoliths revealed a decrease of water flux value after the incorporation of MNPs, from 142 and 294 to 110 and 120 L m^{-2} h^{-1}, respectively. Conversely, AG and DXT monoliths, after MNPs addition, increased the water flux values from 102 and 100 to 212 and 176 L m^{-2} h^{-1}, respectively. This can be explained by morphological features and composition of each support. CHT and CP monoliths, although they exhibit an increase of pore size diameter after MNPs embedding, possess a very well organized 3D porous structure which in wet conditions, behaves homogenously with controlled swelling, namely when confined to a column. After MNPs addition, monoliths stay even better stabilized with a higher water uptake capacity. In a marked contrast, AG and DXT monoliths, which in native conditions already presented high swelling capacity, also exhibit a heterogeneous porous network that hampers a regular profile of water permeation. Furthermore, with the incorporation of MNPs, pores suffer an additional elongation due to MNPs mobility in a random way, and consequently higher water fluxes are achieved. Nevertheless, the obtained values for all supports assure efficient and convenient water fluxes for bioseparation purposes.[11,45]

The compressive mechanical properties were studied by uniaxial compression measurements under dry and hydrated conditions to validate the mechanical resistance of native and magnetic monoliths. In general, higher compression modulus indicate stiffer materials.[46] Concerning the native supports, DXT monoliths are stiffer at dry conditions, followed by CHT, CP and AG monoliths, (Table 1). However, due to their larger pores, DXT in wet state becomes softer (0.6 kPa) while CHT exhibits the highest value of compressive modulus (1.9 kPa). The remaining monoliths present similar values between 0.4–0.7 kPa. The mechanical behavior of CHT in wet conditions is mainly related with its hydrogel nature which excels in the hydrated state. The addition of MNPs to the structures kept the same trend of their mechanical behavior concerning monolith's material, and hydration degree. Additionally, the obtained values are in the range of similar 3D porous structures.[11,42,45]

In order to evaluate the magnetic response of magnetic monoliths, samples in dry and wet conditions, with 1 cm of diameter and height, were placed in contact with different permanent magnets, and the physical deformation (shrinkage) was monitored over time. Figure S1 (see supporting information) shows the magnetic deformation of each support after 20 minutes in contact with permanent magnets with different intensities (0–2.5 T in dry and wet state). In general, independently of the monoliths composition all wet supports presented higher magnetic deformations when compared with the dry states. Although wet monoliths are less stiff, incorporated MNPs offer a higher mobility to all 3D structure allowing a pronounced shrinking. Contrarily, dry magnetic samples are more rigid, therefore the shrinking capacity is inferior or negligible. Another aspect studied was the reversibility of the magnetically induced shrinkage. At low magnetic fields (0.25 and 0.5 T) monoliths have no magnetic memory as they can return to the initial position at both dry and wet conditions (Figure S1, Supporting Information). At 1.5 T the magnetic deformation varies depending on the monolith porous architecture and hydrated state. Thus, CHT_M and AG_M in dry and wet conditions

present magnetic response while CP_M and DXT_M only exhibit it in wet conditions. At 2.5 T all monoliths revealed higher magnetic deformations which led to a total collapse of the 3D porous structures and consequently to the loss of a magnetic reversible response. These observations suggest that a magnetic field of 0.5 T is enough to operate with natural magnetic based monoliths in reversible on-off magnetic cycles without damaging the porous network. All macroporous monoliths were tested over four ON-OFF cycles at 0.5 T and always maintained their superparamagnetic behavior, that is, reversible magnetic response and absence of magnetic memory.

In view of the application of magnetic monoliths for bioseparation purposes, iron leaching is an important issue to address. Leaching of MNPs was investigated at different conditions employed in typical Ab purification processes mainly during the cleaning and regeneration steps. Figure S2 (see Supporting Information) shows MNPs leaching profiles from different natural magnetic based monoliths over time (12 h). In general, MNPs leaching is negligible since the highest values achieved were around 4–6% at pH 5 after 4 h, and between 4 and 9% upon contact with alcohols, after 1 h. Chitosan has a pKa around 6–6.5 and at pH 5, chitosan based-structures exhibit high swelling capacity (porous network opening) which justifies the accentuated MNPs leaching. In addition, although agarose and dextran are uncharged polysaccharides, the acrylamide presented in monoliths composition has a NH_2 group with a pKa value around 6, which, due to the same reason previously mentioned, leads to high MNPs release at pH 5. DXT_M was the most unstable support since, except for regeneration buffer and NaOH solution, the MNPs leaching is higher. Nevertheless, in general, all supports presented negligible MNP leaching at the conditions (buffer and time of exposition) typically employed in a purification protocol.

2.2. Preparation and Characterization of Hybrid Monoliths

Magnetic monoliths were functionalized with an affinity ligand resulting in a hybrid material. The affinity ligand employed in this work was the small synthetic molecule TPN-BM previously developed in our groups and which presents affinity towards IgG.[40] The immobilization of functional molecules onto polymeric materials surfaces requires the presence of active chemical groups as primary amines.[47] Plasma technology was the selected tool to fulfil this requirement in a green and sustainable way as it allows diverse solvent free modifications on supports within short periods.[38,39,48] Firstly, free radicals were generated under inert-gas discharge environments at the surface of selected monoliths, followed by a second step reaction in which 1,6-hexanediamine was dragged under vacuum (in situ) to react with the activated supports for further ligand coupling (**Figure 2**A). As shown in Figure 2B, large densities of amines were introduced in all magnetic supports, particularly in CHT_M (460 ± 44 µmol of NH_2 per gram of support). The application of plasma technology for the activation and amination of monoliths saved time and solvents consumption when comparing with traditional procedures applied for the same purpose.[29,49] In this work, 30 min were sufficient to aminate

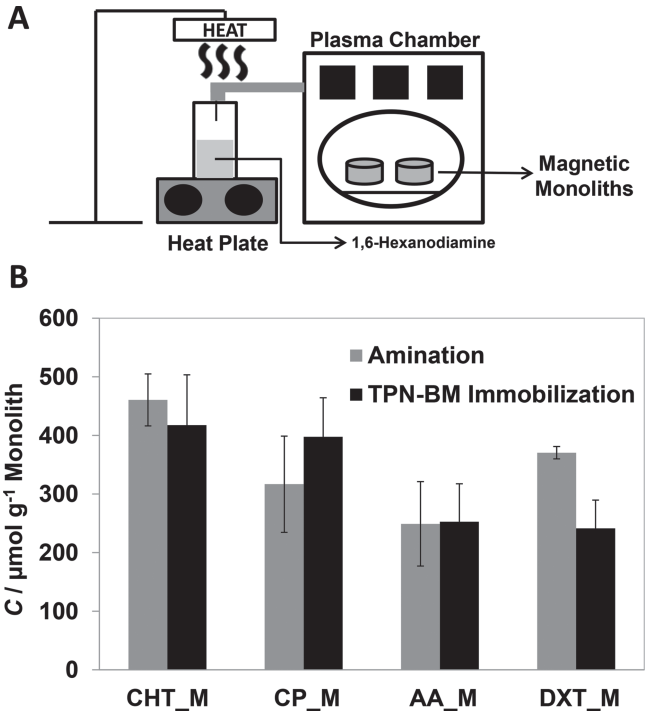

Figure 2. Schematic representation of: A) the amination procedure, assisted by plasma technology, of magnetic natural-based monoliths. B) Graphical representation of the amination and TPN-BM immobilization yields obtained for all magnetic monoliths.

the supports in contrast with the typical 13 h needed in the traditional approach (1 h for epoxyactivation plus 12 h for amination).[1] Aminated monolithic platforms were subsequently functionalized with ligand TPN-BM. Different yields of ligand immobilization were reached according with the previous amination levels (Figure 2B). The highest immobilization value of TPN-BM was obtained for CHT_M and DXT_M monoliths (around 400 µmol TPN-BM g^{-1} support) followed by CP_M, and AG_M (370 and 280 µmol TPN-BM g^{-1} support, respectively). The results from ligand immobilization suggest that most amines reacted with TPN-BM turning the present immobilization strategy extremely effective. After TPN-BM immobilization all magnetic supports were again characterized.

SEM images presented in Figure 1F and I show that the porous networks of hybrid CP and AG monoliths (CP_M_TPN-BM and AG_M_TPN-BM respectively) were maintained after the functionalization procedure. Contrarily, hybrid CHT and DXT monoliths (CHT_M_TPN-BM (Figure 1C) and DXT_M_TPN-BM (Figure 1L) respectively) exhibited morphological differences, namely pore enlargement and deformated coiled pores, respectively. In addition, all monoliths present an increase in pores thickness which might be indicative of ligand attachment. Differences regarding average pore size diameter, porosity and surface area values of supports after ligand coupling were also registered (**Table 2**). The CHT_M_TPN-BM registered an increase in average pore size diameter (from 89 to 125 µm) while the remaining registered a 3-fold decrease of the pore size. After TPN-BM coupling, all monoliths revealed a

Table 2. Morphological and mechanical characterization of hybrid monoliths. All data was obtained from duplicated and triplicated measurements.[a)] Determined for dried monoliths by mercury porosimetry analysis.

		CHT_M_TPN-BM	CP_M_TPN-BM	AG_M_ TPN-BM	DXT_M_TPN-BM
Average pore size diameter [μm][a)]		125 ± 5	20 ± 5	18 ± 5	13 ± 5
Porosity [%][a)]		79 ± 9	75 ± 9	76 ± 5	61 ± 5
Water Flux [L m^{-2} h^{-1}]		176 ± 9	135 ± 8	186 ± 9	78 ± 5
Surface Area [m^2 g^{-1}][a)]		1.4 ± 0.2	1.1 ± 0.2	2.9 ± 0.2	3.4 ± 0.2
Compressive Modulus [kPa]	Dry	0.3 ± 0.1	191 ± 9	0.5 ± 0.2	0.7 ± 0.4
	Wet	0.2 ± 0.1	55 ± 5	0.5 ± 0.2	0.3 ± 0.2

higher rigidity and, in dry conditions used during MIP analysis, the pores are more collapsed turning hard the mercury intrusion porosimetry. Porosity and surface area values kept close to the ones obtained before functionalization. The water flux values decreased for all supports which can be explained by the hydrophobic nature of TPN-BM. Still, all monoliths exhibited acceptable water uptake capabilities that assure the permeation of Ab or other large biomolecules. The compressive modulus of CHT_M_TPN-BM and DXT_M_ TPN-BM decreased, which is in agreement with the enlargement and winding of the porous network upon functionalization, since larger pores and high porosities led to soft materials.[46] Conversely, CP_M_TPN-BM became stiffer in dry and wet conditions (≈20-fold comparing to non-functionalized supports) which are in accordance with the pore size decrease. AG_M_TPN-BM maintained their mechanical behavior. In addition all supports were tested for magnetic response under a magnetic field of 0.5 T. All monoliths maintained the deformation in both states, dry and wet, as before ligand coupling, except for CP_M_TPN-BM which lost magnetic response in dry condition.

Also the surface chemical composition of hybrid monoliths CP_M_TPN-BM and AG_M_TPN-BM was analysed by XPS. For control, the corresponding aminated and non-aminated versions (CP_M_Amine, AG_M_Amine, CP_N and AG_N, respectively) were analysed and compared. Detailed XPS regions C 1s, N 1s, and Fe 2p are shown in **Figure 3**A) – F). In CP_N

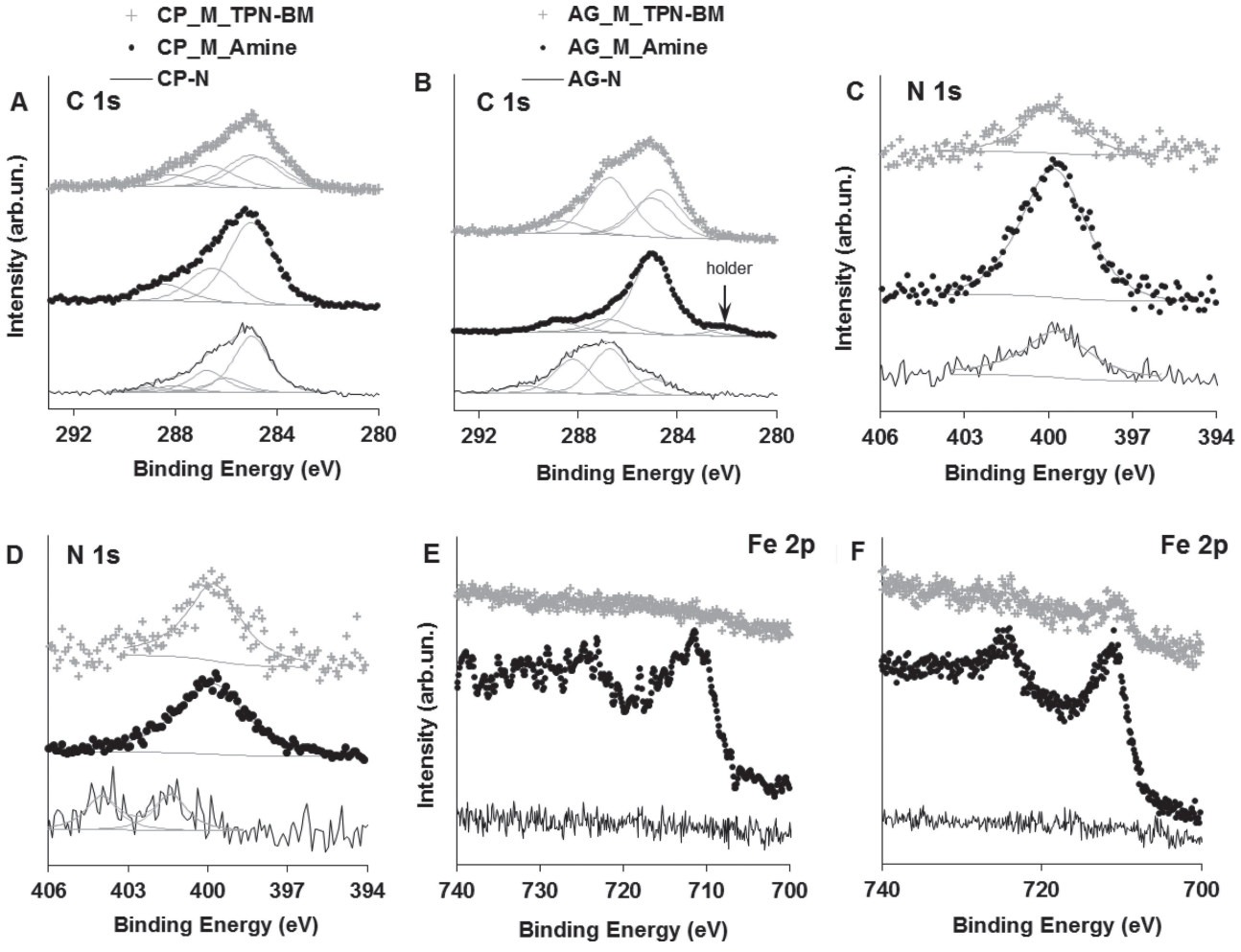

Figure 3. XPS regions C 1s, N 1s, and Fe 2p of native monoliths (black), magnetic and aminated (green) and hybrid monoliths (blue).

besides the aliphatic carbons at a binding energy (BE) of 285 eV from PVA, C 1s also includes peaks centred at 286.0, 286.7, and 288.2 eV assigned mainly to chitosan carbons C–N, C–O, and O–C–O, respectively.[50] Carbon singly bound to oxygen also exists in PVA and the peak at 286.0 eV can also include the contribution of C-N from the cross-linker (MBA), as attested by the peak centred at 288.8 eV attributed to N-C = O from MBA.[50] The C 1s region of agarose-based native monolith, AG_N, was fitted with four peaks centred at 285, 286.7, 288.2, and 290.2 eV. The most intense peak (at 286.7 eV) corresponds mostly to C–O in agarose, the peak centred at 288.2 eV includes not only agarose O–C–O carbons, but also N–C=O from acrylamide and/or the MBA cross-linker, whose existence is attested by the presence of nitrogen. Finally, the peak centred at higher BE can be attributed to carbon in a very electronegative neighbourhood such as a carbonate for instance, however since carbonates are not likely to exist in this system, this shifted peak is compatible with a differential charge effect, that is, it can correspond to carbon atoms in a phase with a loose electrical contact with the other phase, revealing an heterogeneous sample. In both native monoliths (which are composed by chitosan or agarose entrapped by synthetic polymers (see Figure S3 in Supporting Information)) the XPS N 1s regions include the contribution of amines and amides. Even in the presence of MNP and after functionalization with diamines and diamines followed by the ligand (TPN-BM), just one single peak centred at 399.8 eV was fitted. In fact, this peak can be the sum of different nitrogen atoms (in samples with ligand it can also include aromatic N), regardless the different chemical neighbourhoods.[50] The only exception is N 1s of AG_N that shows two narrower peaks slightly shifted to higher BE which is most probably due to a differential charge effect already suspected in C 1s region.

A large decrease of iron was observed since Fe 2p region is rarely or not detected in functionalized samples, revealing an efficient coating of the MNPs. However, in aminated samples iron was detected. Fe $2_{p3/2}$ has three peaks, centred at 709.3, 711.1 and 713.4 eV, assigned to Fe^{2+}, Fe^{3+} in oxide (Fe_2O_3) or oxyhydroxide (Fe(OH)O) and iron in a very electronegative environment superimposed to a multiplet structure typical of Fe^{2+} oxides, respectively.[51,52] Also the quantitative results were gathered in **Table 3**.

Comparison of monoliths containing MNPs show that the MNPs were effectively embedded in the polymer matrix since upon functionalization with TPN-BM, the XPS atomic ratio Fe/C decreased (becoming almost zero when the ligand is present). Moreover, comparing CP_M_TPN-BM and AG_M_TPN-BM, it is also evident that MNPs coating with polymer/amine/TPN-BM is more efficient in the CP-based hybrid (where the Fe/C ratio in the aminated monolith is lower and decreases to values that were not quantifiable when the ligand TPN-BM was added) than in the AG-based one. Additionally, the XPS N/C atomic ratio is larger in aminated monoliths than in the native ones, showing that in fact, the monoliths were efficiently modified with 1,6-hexanodiamine through the functionalization strategy based on plasma technology. Also, the N/C ratio is larger in aminated monoliths than in the monoliths subsequently functionalized with the ligand TPN-BM. This parameter, again, confirms that the more superficial layer is, in fact, the TPN-BM since the stoichiometric ratio N/C in di-hexamine is 1/3 whereas in the ligand (TPN-BM) is 3/19. However, a more quantitative analysis is not possible since samples are stratified whereas the

Table 3. Binding Energies (eV) ± standard deviations and quantitative results obtained for chitosan/poly(vinyl alcohol) (CP) and agarose based-monoliths (AG) in native (N), magnetic (M), aminated (A), and hybrid (TPN-BM) conditions.

XPS peak (BE, eV)	AG_M_TPN-BM	AG_M_Aminated	N-AG	CP_M_TPN-BM	CP_M_Aminated	N-CP
C 1s (284.7 ± 0.1)	20.6	n.o.	n.o.	21.8	n.o.	n.o.
C 1s (285.0 ± 0.1)	16.8	48.6	10.5	23.0	38.0	36.2
C 1s (286.0 ± 0.1)	n.o.	n.o.	n.o.	n.o.	n.o.	9.0
C 1s (286.7 ± 0.1)	24.7	8.3	29.3	14.9	15.9	13.7
C 1s (288.2 ± 0.2)	n.o.	n.o.	22.0	8.2	7.9	4.1
C 1s (288.8 ± 0.1)	5.4	6.4	n.o.	n.o.	n.o.	3.0
C 1s (290.2 ± 0.1)	n.o.	n.o.	4.9	n.o.	n.o.	n.o.
O 1s (530.4 ± 0.1)	4.4	9.4	n.o.	n.o.	n.o.	n.o.
O 1s (531.7 ± 0.3)	n.o.	137	6.6	8.1	26.5	5.9
O 1s (533.1 ± 0.5)	23.7	5.5	23.1	19.3	n.o.	20.9
N 1s (399.8 ± 0.1)	4.1	6.6	n.o.	4.8	10.5	7.3
N 1s (401.4 ± 0.1)	n.o.	n.o.	1.9	n.o.	n.o.	n.o.
N 1s (404.0 ± 0.1)	n.o.	n.o.	1.8	n.o.	n.o.	n.o.
Fe $2p_{3/2}$ (709.3 ± 0.2)	0.1	0.3	n.o.	n.o.	0.5	n.o.
Fe $2p_{3/2}$ (711.1 ± 0.3)	0.2	0.9	n.o.	n.o.	0.5	n.o.
Fe $2p_{3/2}$ (713.4 ± 0.4)	0.1	0.4	n.o.	n.o.	0.4	n.o.
Atomic Ratios						
Fe/C	0.007	0.026	n.o.	n.o.	0.021	n.o.
N/C	0.06	0.10	0.06	0.07	0.17	0.11

n.o.: not observed.

ratios computed from XPS assume a homogeneous composition in depth.

The leaching of ligand TPN-BM was also evaluated for all hybrid supports, under the same conditions tested for MNPs leaching. Once again, considering the time of exposure to the harsh conditions tested (supports are never exposed more than 1 hour to each buffer), the monoliths stability is assured except for DXT_M_TPN-BM (Figure S4, Supporting Information).

2.3. Hybrid Monoliths in Ab purification

Once completely characterized and evaluated, magnetic and hybrid monoliths were submitted to static partition equilibrium measurements with hIgG and BSA (a model contaminant protein), in order to estimate the maximum binding capacity to the target molecule (hIgG) as well as the level of non-specific adsorption (BSA). The experimental data was fitted using a Langmuir–Freundlich isotherm considered to be the indicated for porous structures with heterogeneous morphology and already applied with success in similar supports.[53,54] **Figure 4** exhibits the adsorption profiles while **Table 4** shows the different affinity constants (K_a), theoretical maximum capacities (Q_{max}) and Langmuir–Freundlich coefficients (n) estimated. Considering the studies involving hIgG, the controls always exhibit lower K_a, Q_{max}, and n values comparing with the functionalized ones. This observation suggests that the addition of TPN-BM ligand to the magnetic supports increases their specificity towards hIgG. Concerning the experiments with BSA, very few differences between magnetic and hybrid monolithic samples were found, suggesting that TPN-BM ligand coupling does not affect BSA adsorption and consequently, no affinity for BSA is manifested as expected. In order to explore dynamic binding and mass transfer properties for the hybrid monoliths, breakthrough curves of pure hIgG solutions were estimated in duplicate (**Figure 5**). Protein recovery was estimated using pH 3.0 (**Figure 6**A) and pH 11.0 (Figure 6B) buffers. Elution buffer with pH 3.0 proved to be efficient for IgG recovery when ligands 22/8 and TPN-BM were coupled onto CHT and CP monoliths.[11,49] On the other hand, pH 11.0 buffer demonstrated to be the best elution condition for MNPs functionalized with the affinity ligand 22/8.[29]

Regarding the monoliths capacity, DXT_M_TPN-BM monolith presented the poorest scenario since it was able to capture 80 mg

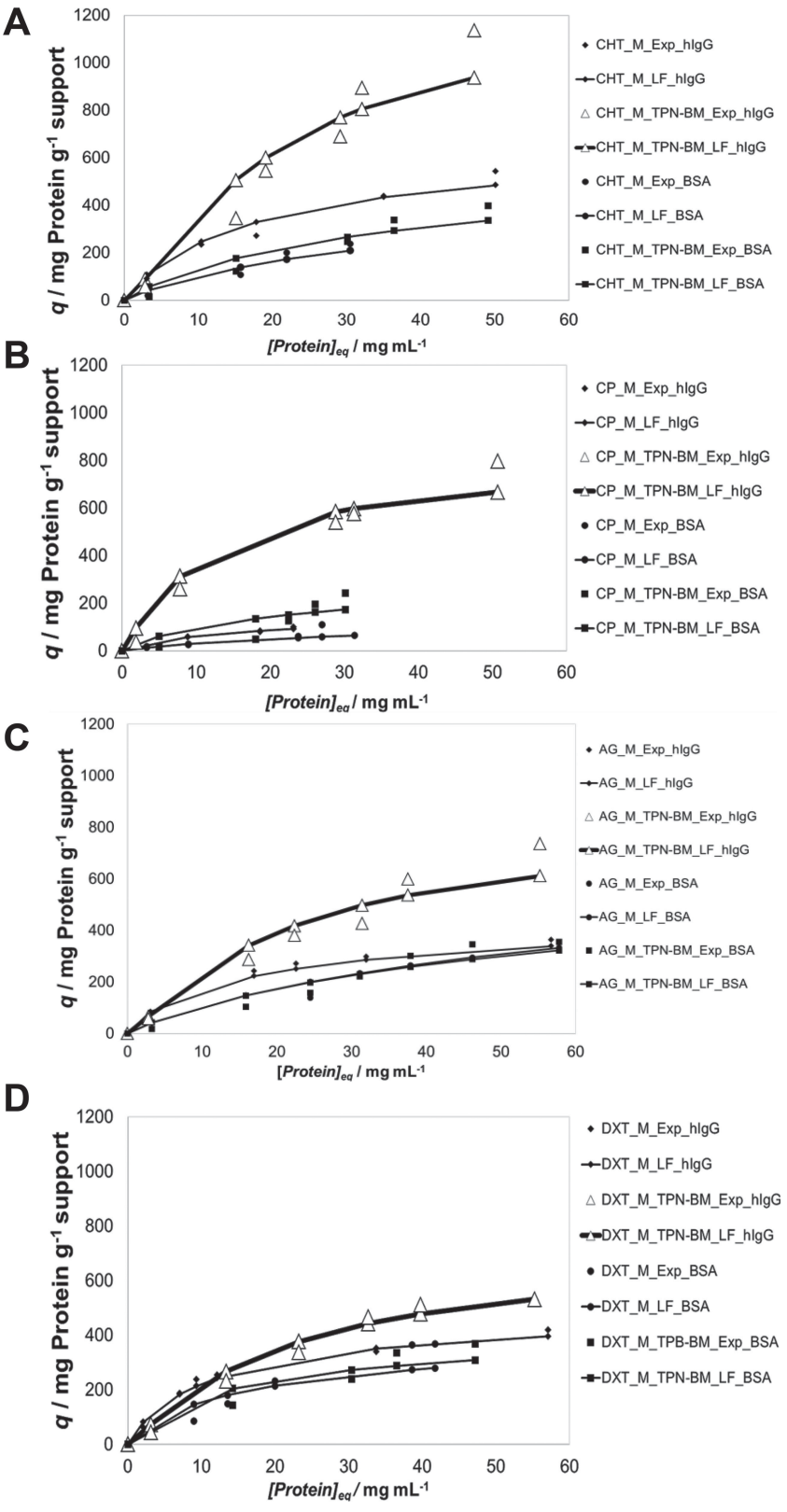

Figure 4. Graphical representation of experimental adsorption isotherms (Exp) fitted by Langmuir-Freundlich (LF) model for magnetic (M) and hybrid (M-TPN-BM) monoliths: A) CHT_M and CHT_M_TPB-BM, B) CP_M and CP_M_TPN-BM, C) AG_M and AG_M_TPN-BM, D) DXT_M and DXT_M_TPN-BM.

Table 4. Summary of the estimated parameters of the Langmuir–Freundlich isotherms for all magnetic and hybrid monoliths.

	K_a/ [10^4 M^{-1}]		Q_{max} [mg g^{-1} support]		n	
hIgG	Control	TPN-BM	Control	TPN-BM	Control	TPN-BM
CHT_M	0.9	3.0	600	1400	0.9	1.3
CP_M	1.2	2.0	180	800	0.8	1.2
AG_M	1	3.0	500	800	0.8	1.3
DXT_M	0.2	4.0	500	700	0.9	1.2
BSA						
CHT_M	0.2	0.2	550	600	0.9	0.9
CP_M	0.3	0.2	100	200	0.8	0.8
AG_M	0.2	0.2	625	665	0.8	0.9
DXT_M	0.6	0.5	450	450	0.8	0.8

hIgG per gram of support. Nevertheless, CHT_M_TPN-BM, CP M_TPN-BM and AG M_TPN-BM monoliths exhibited better values of hIgG retention translated by appreciable values of binding (100, 99, and 103 ± 10 mg hIgG g^{-1} support, respectively). Considering the elution profile, DXT_M_TPN-BM monolith showed a lower hIgG recovery (28% of total hIgG bound at pH 3 and 14% of total hIgG bound at pH 11), as opposed to CHT_M_TPN-BM, CP M_TPN-BM and AG M_TPN-BM (73, 77 and 63 ± 7%, respectively). In addition, elution at pH 3 revealed better values compared to those obtained at pH 11.

In order to assess the effect of magnetic deformation for a better recovery yield, a tailored permanent magnet was designed. This was performed taking into consideration that: 1) the magnet needs to provide the required magnetic effect on the monolith and, 2) its shape needs to help the extraction of antibody from the monolith by mechanical shrinking. In order to satisfy point (1), a FEM parametric analysis led to the magnet optimal shape (Figure S5, see Supporting Information) and the magnetic material adopted was neodymium 52, N52, (1.44 T of magnetic remanence). For point (2), a geometrical constraint was fixed: the need to have a straight-hole magnet shape, with a diameter of 11 mm, i.e. the diameter of the monolith housing. Thus, in a typical chromatographic operation, the loading of the sample is performed in the absence of magnetic field assuring that all pores of monoliths are completely available to process the proteins extract without blocking. The same happens during the washing step, where unspecific bound proteins are removed. The elution step is performed in the presence of the tailor-made magnet as to induce a mechanical deformation onto the hybrid monoliths (Figure 5A). The elution capacities (at pH 3.0) for all hybrid supports in the presence and absence of magnetic field are shown in Figure 5B. After charging the monolithic supports with pure hIgG (1 mL) of solution (2 mg mL^{-1}), it was possible to accomplish a faster recovery of 15% more hIgG under a magnetically-assisted elution as compared to the elution achieved in the absence of magnetic field. CP_M_A and AG_M_A monoliths revealed higher binding capacities and an elution capability of 90 ± 5% when assisted by a magnetic field. Moreover, the magnetically-assisted elution takes half time (≤30 s) than a normal elution, which is also a great benefit in terms of time consumption. In addition, the protein is exposed during less time to the low pH of the elution buffer, which decreases protein deterioration and aggregation.In order to evaluate the re-use capability of the hybrid monoliths, three consecutive chromatographic cycles and a fourth one after monolith autoclaving (After_AC) were performed, in duplicates, at an approximate flow rate of 1 mL min^{-1} (**Figure 7**). The DXT_M_TPN-BM monolith was not tested due to its fragile appearance and weak performance. Over four cycles, CHT_M_TPN-BM, CP M_TPN-BM and AG M_TPN-BM monoliths displayed a similar profile of binding, magnetically-assisted elution and regeneration, suggesting a reproducible behavior in the capture and recovery of hIgG. CP M_TPN-BM monolith showed to be the most promising one since its binding capacity achieved 125 ± 15 mg hIgG g^{-1} support, followed by AG M_TPN-BM (115 ± 10 mg hIgG g^{-1} support) and CHT_M_TPN-BM (90 ± 13 mg hIgG g^{-1} support). Concerning the efficiency of hIgG recovery, CP M_TPN-BM monolith remains the best one since it is able to release 90 ± 5% of the total hIgG bound, and only 8 ± 5% is removed from the support during the regeneration step. AG M_TPN-BM monolith also registered a promising elution profile translated by the recovery hIgG (88 ± 4%). The lowest performance was verified for CHT_M_TPN-BM monolith since it was only possible to recover 70 ± 8% of hIgG bound, remaining 30 ± 2% of hIgG in the support that was only excluded in the regeneration step. Magnetic monoliths (control) were also tested but only approximately 25 mg of IgG per gram of support were retained. In the elution and regeneration steps the amount of IgG retained was completely recovered.

The most challenging issue was to evaluate the selectivity of the hybrid materials for mAbs purification. As CP_M_TPN-BM and AG_M_TPN-BM monoliths revealed encouraging chromatographic profiles, they were selected to proceed with the purification of mAbs directly from unclarified crude extracts. **Figure 8** summarizes the total amount of protein captured and eluted from both supports, at different magnetically-assisted elution conditions (pH 3 and 11) (A) as well as the respective SDS-PAGE gels (B). Considering the binding capacity, both supports revealed similar performance (17 ± 5 mg total protein per gram of monolith) however, clear differences are visible in the elution capability. CP_M_TPN-BM exhibits the highest elution value (98% of total protein bound) at pH 3 while AG_M_TPN-BM monolith achieved the same value but at pH 11. In order to evaluate the purity of the fractions, SDS gels were performed (Figure 8B and C). CP_M_TPN-BM (Figure 8B) and AG_M_TPN-BM (Figure 8C) monoliths showed high selectivity for mAbs: the elution fractions (lanes 7, 8, 9, and 10) presented only the bands of mAbs fragments (50–25 kDa) yielding a purity of approximately 97% (estimated by ImageJ analysis). All other contaminants were excluded in the washes (lanes 4, 5, and 6). These results suggest that CP_M_TPN-BM and AG_M_TPN-BM are promising supports for Ab recognition and isolation. CP_M and AG_M monoliths (control) revealed no affinity for mAbs capture.

3. Conclusions

The use of antibodies and derivative structures as effective therapeutics for cancer, autoimmune, infectious and inflammation

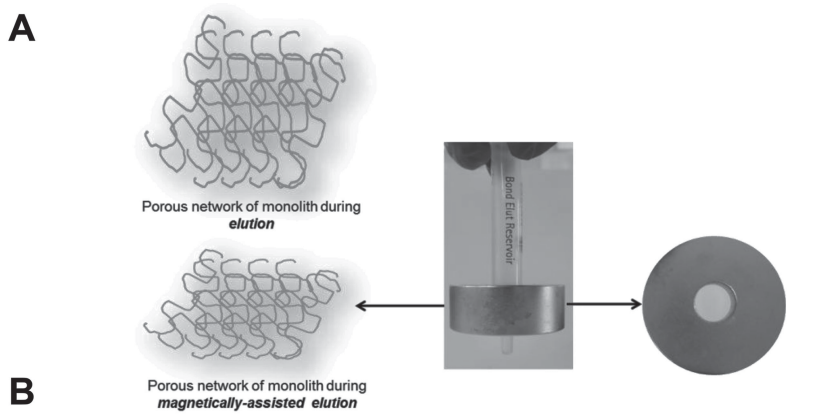

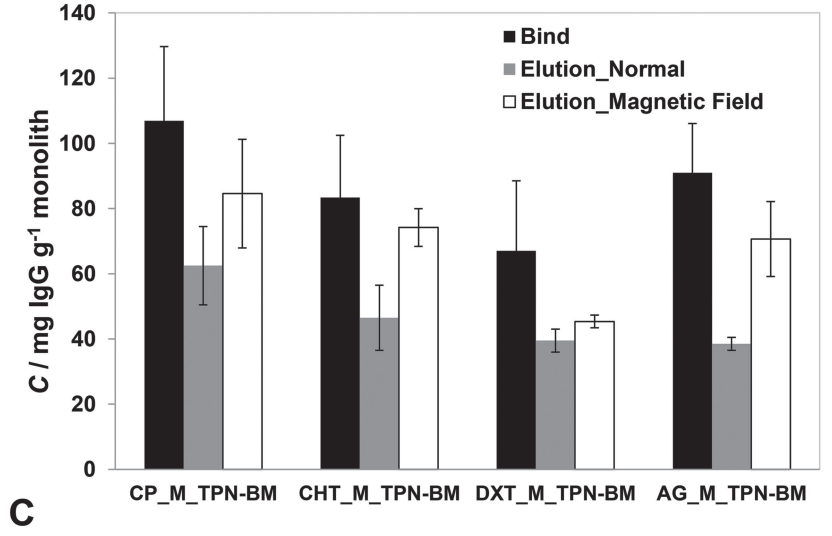

C

Support	Bind (mg IgG g^{-1} support)	Normal Elution (mg IgG g^{-1} support)	Magnetic Elution (mg IgG g^{-1} support)
CP_M_TPN-BM	106±22	63±12	85±16
CHT_M_TPN-BM	83±19	47±10	74±6
DXT_M_TPN-BM	67±21	40±5	45±3
AG_M_TPN-BM	91±15	38±3	71±11

Figure 5. A) Schematic representation of the porous network availability of hybrid monoliths during typical and magnetically-assisted elution of chromatographic experiments. B) Graphical representation of binding (black), normal elution (grey) and magnetically-assisted elution (white) of hybrid natural-based monoliths. C) Values for the binding and elution (conventional and magnetically-assisted) of IgG from the monolithic supports developed in this work.

diseases increased exponentially with an annual market worth tens of billions of US dollars. Thus, in order to give an answer to such demand, we report the preparation of hybrid materials for Ab purification. These materials based on natural polymers were prepared in such a way that macroporous networks with great morphological and mechanical properties were created. Magnetic nanoparticles were embedded and an artificial ligand mimicking Protein A (TPN-BM) was coupled into the monoliths, endowing hybrid characteristics. The functionalization with TPN-BM conferred selectivity to the supports while the MNPs incorporation increased and accelerated Ab recovery. Green and solvent free strategies were employed to prepare and modify the hybrid monoliths, namely freeze-drying method and plasma technology.

The presented hybrid platforms distinguish from others previously reported due to three main aspects: 1) they were prepared following the metrics of green chemistry in order to save solvents, time and energy consumption, and designed for degradation; 2) they gather in just one material two main properties, affinity and magnetic response, and 3) they allow an efficient and fast operation, as the magnetic response facilitates the release of the target molecule that is typically performed under drastic acidic or basic pH. The hybrid materials also exhibited a considerable stability towards CIP and SIP which underline their robustness.

The magnetically-assisted elution process was efficient, faster and selective for Ab purification since CP_M_TPN-BM and AG_M_TPN-BM monoliths were able to bind 120 ± 10 mg of hIgG per gram of monolith and to elute 91 ± 5% for at least four consecutive cycles. Moreover, when tested with crude samples, both supports showed a good specificity for mAbs, recovering them with 97% of purity. When compared with affinity chromatography purification protocols employing protein A resins,[58] the systems presented in this work showed higher binding capacities (120 mg IgG g^{-1} support as compared to 10 mg mL^{-1}). Protein A resins are described to withstand over 100 cycles of purification—our system was tested only over 4 cycles and therefore it is not possible to extrapolate the behavior for such long periods of usage. However, this effect can be compensated by the low cost, high biodegradability and disposable potential of the materials employed in monoliths preparation.

The hybrid structures and the magnetically-assisted elution can be easily extended to the recognition and separation of different biomolecules with high added value by changing only the immobilized ligand. In addition, the application of these systems in biosensing or biomedical devices is also envisaged.

4. Experimental Section

Materials: Ammonium persulfate (APS, purity ≥ 98%), citric acid (purity ≥ 99%), disodium hydrogen phosphate monodibasic (pa), disodium hydrogen phosphate dibasic (pa), disodium tetraborate, ethanol absolute and sodium citrate dihydrate were purchased from Merck. Isopropanol and sodium bicarbonate were purchased from Riedel-de-Haën. Agarose (electrophoresis grade) was purchased from Nzytech. Acetone (purity ≥ 99%), and ethyl acetate were supplied by Roth. Acetic

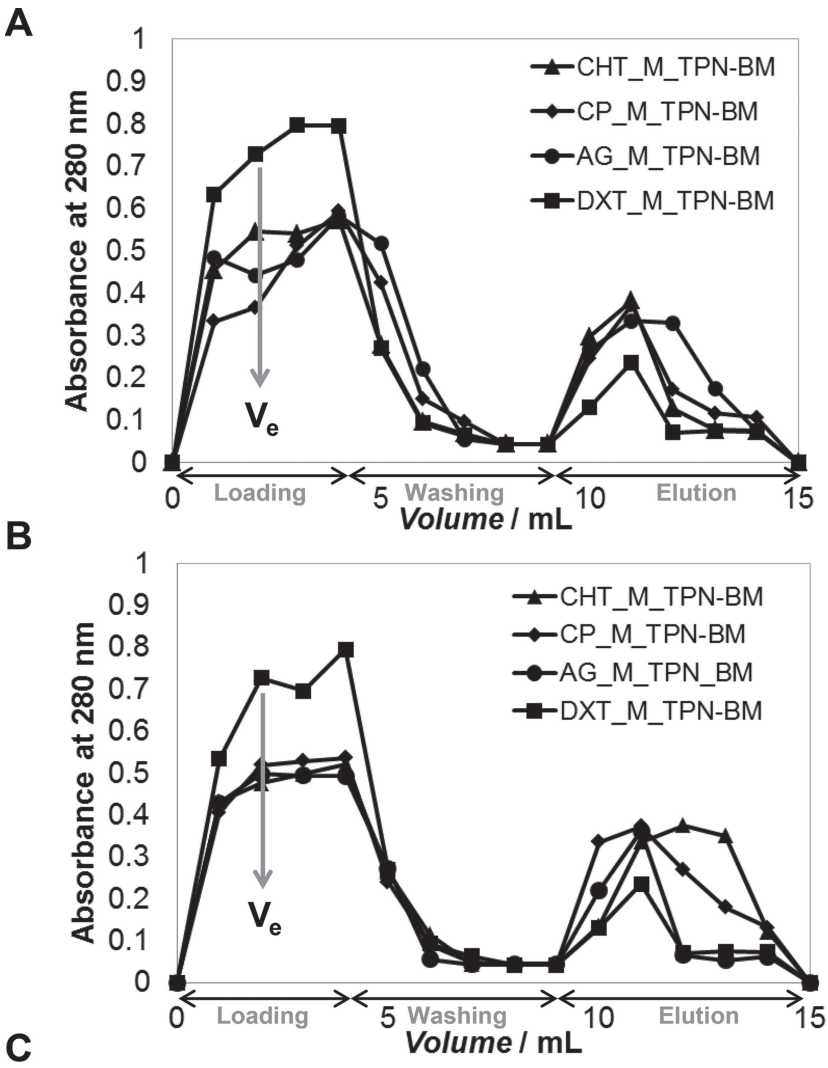

C

	Binding (mg hIgG g^{-1}support)	Elution at pH 3 % (mg hIgG g^{-1} support)	Elution at pH 11 % (mg hIgG g^{-1} support)
CHT_M_TPN-BM	100±10	73±3	42±15
CP_M_TPN-BM	99±12	77±10	65±10
AG_M_TPN-BM	103±10	63±12	45±5
DXT_M_TPN-BM	80±7	28±5	14±3

Figure 6. Breakthrough profiles for human IgG upon CHT_M_TPB-BM (▲), CP_M_TPN-BM (◆), AG_M_TPN-BM (●) and DXT_M_TPN-BM (■) monoliths, performing the elution at A) pH 3 and B) pH 11. C) Summary of the binding and elution capacities estimated through breakthrough curves at different elution conditions.

acid (purity ≥ 99%), aminocaproic acid, 3-aminophenol, 4-amino-1-naphthol hydrochloride, cyanuric chloride (purity ≥ 98%), 1,6-hexanediamine (purity ≥ 98%), N,N-dimethylformamide (DMF), dimethylsulfoxide (DMSO), chloridric acid (HCl), glycine, ninhydrin, iron (II) chloride tetrahydrate ($FeCl_2.4H_2O$, purity ≥ 99%), iron (III) chloride hexahydrate ($FeCl_3.6H_2O$, purity ≥ 99%), potassium cyanide, pyridine, sodium hydroxide (purity ≥ 99%), sulfuric acid (H_2SO_4, purity ≥ 95%), sodium phosphate monobasic monohydrate ($H_2NaO_4P.H_2O$, purity ≥ 98%), di-sodium hydrogen phosphate 2-hydrate ($Na_2HPO_4.2H_2O$, purity ≥ 98%) were purchased from Sigma Aldrich. Acrylamide (C_3H_5NO, purity ≥ 99%), anthrone ($C_{14}H_{10}O$, purity ≈ 97%), ammonium hydroxide (NH_4OH, 5.0N) chitosan (75~85% deacetylated, medium molecular weight), dextran (($C_6H_{10}O_5$)n), hydroxylamine hydrochloride ($H_3NO.HCl$, purity ≥ 99%), poly(vinyl alcohol) (purity ≈ 99%), *N,N*-methylenebisacrylamide (MBAm, purity ≥ 85%), *N,N,N′,N′*-tetramethylethylenediamine (TEMED, purity ≈ 99%), bicinchoninic acid (BCA) kit, bovine serum albumin (BSA) (purity ≥ 98%) were supplied by Sigma Aldrich. Human IgG (Gammanorm) was supplied by Octapharma (purity ≥ 99%). 1.10-phenonthroline 1-hydrate ($C_{12}H_8N_2.H_20$, purity ≈ 99%) was acquired from Panreac.

Preparation of Magnetic Nanoparticles (MNPs): Magnetic nanoparticles were synthesized via alkaline precipitation of $FeCl_3$ and $FeCl_2$ using a Fe^{2+}/ Fe^{3+} molar ratio of 0.5, according to Batalha et al.[29] In a sealed stirred reactor with agitation at approximately 1200 rpm, ammonium hydroxide (250 ml, 0.7 M) in deionized water was purged with N_2 during 30 min. Then, a freshly prepared iron solution (5.4 g of $FeCl_3.6H_2O$ and 2.0 g of $FeCl_2.4H_20$ in 25 mL of deionized water) was added dropwise. The reaction occurred for 2 h under an inert atmosphere. The pH was maintained at 10 by the addition of ammonium hydroxide. At the end, the particles were washed five times with deionized water by magnetic separation. MNPs were characterized by dynamic light scattering (DLS) and a diameter of 384 ±19 nm was obtained with a polydispersity (PI) of 0.97 ± 0.11.

Evaluation of Polymers Adsorption on MNPs: The evaluation of polymers adsorption on MNPs was performed in order to determine the ratio of MNPs-polymer necessary to prepare stable porous structures with low MNPs leaching events. The adsorption capacity of chitosan, dextran and agarose onto MNPs was studied by static partition equilibrium experiments. MNPs (10 mg, 10 mg mL^{-1}) were incubated with various solutions of polymers (0–15 mg mL^{-1}) prepared in deionized water (agarose and dextran) and in acidic deionized water (1% v/v) (chitosan). All experiments were performed in duplicates at 80 °C, as this is the temperature employed for polymers solubilisation, at 200 rpm for 24 h. At the end, MNPs were removed from the medium by magnetic separation and the amount of adsorbed polymer was determined by the anthrone method.[55]

Preparation of Native and Magnetic Monoliths: Native monoliths were prepared in 4 steps. 1) Chitosan (90 mg), agarose (70 mg) and dextran (70 mg) were dissolved in deionized water 1% (v/v) acidic (3 mL) only for chitosan-based casting solutions. In order to improve the mechanical properties of monoliths, for agarose and dextran casting solutions acrylamide (10 mg) and of GMA (10 µL) were added. In case of chitosan a new casting composed of chitosan (45 mg) and PVA (45 mg) was prepared as described by Barroso et al.[11] 2) The crosslinker agent, MBA, was also added (2% (wt per wt)) to the casting solutions, which were further placed in glass tubes (1 cm of diameter and 3 cm of height) and stirred at 80 °C to assure homogeneous solutions. 3) After

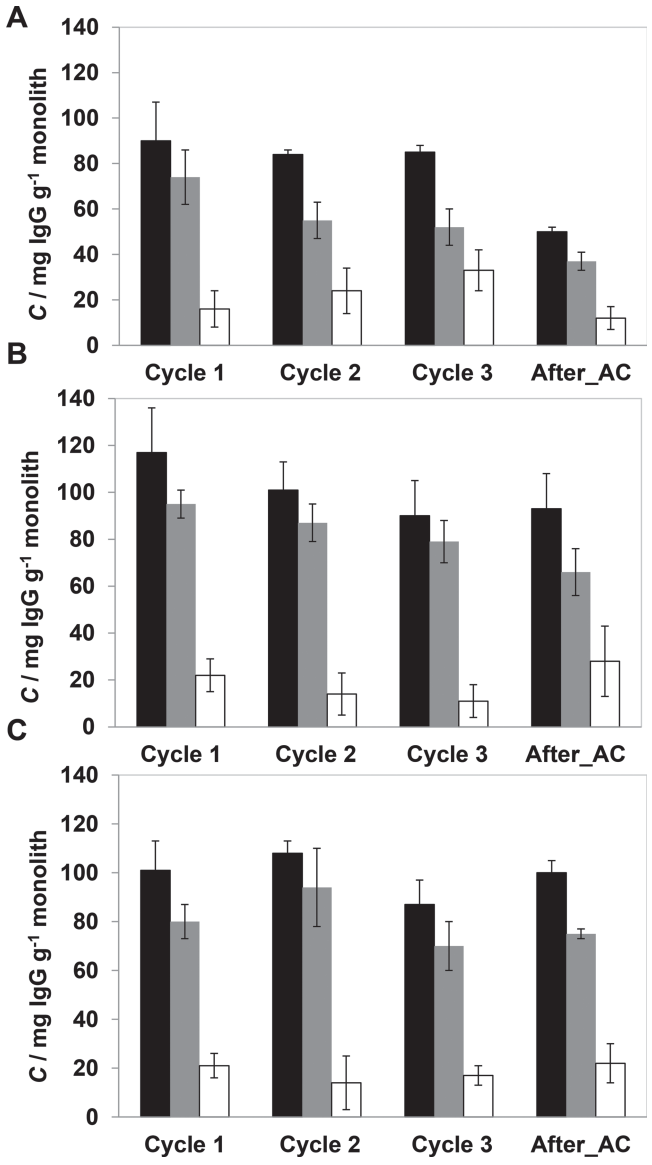

Figure 7. Evaluation of chromatographic performance of A) CHT_M_TPN-BM, B) CP_M_TPN-BM, and C) AG_M_TPN-BM monoliths using pure IgG solutions. The chromatographic procedures, bind (black), elution (grey) and regeneration (white) steps, were performed consecutively along four cycles at a flow rate of 1 mL min^{-1}. The last cycle was performed after autoclaving (After_AC). The elution was assisted by the permanent magnet (0.5 T).

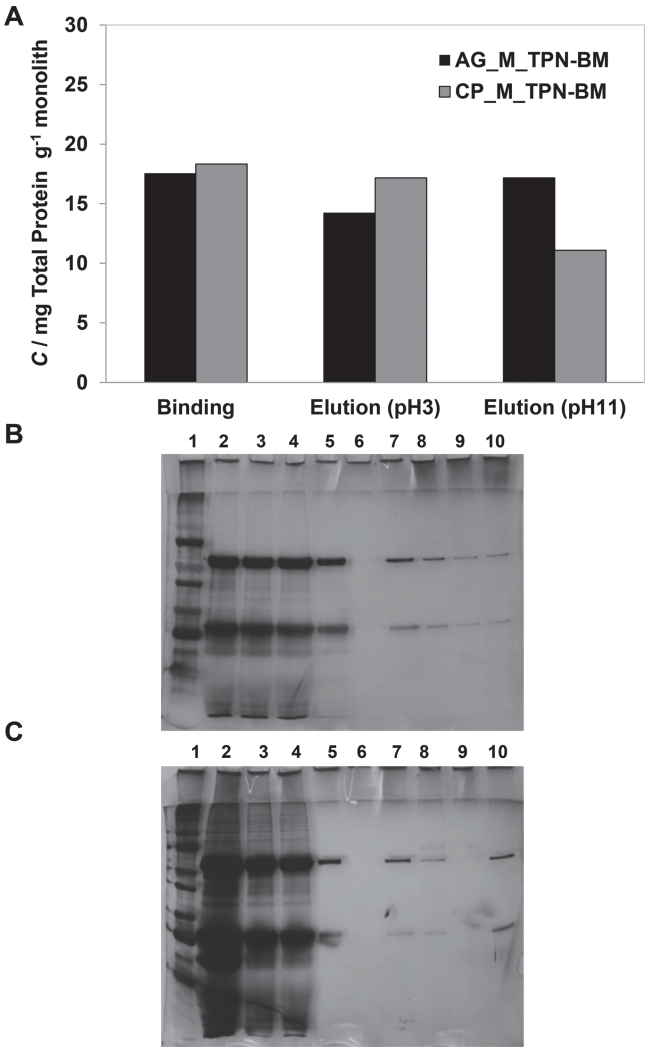

Figure 8. Chromatographic performance of CP_M_TPN-BM and AG_M_TPN-BM in mAbs purification from a non-heterogeneous crude sample with an associated error of ± 5.0. A) The acrylamide gel from SDS- PAGE performed with the fractions collected during the mAbs purification using CP_M_TPN-BM and AG_M_TPN-BM (B and C) at the best conditions of elution: lane 1 corresponds to the molecular weight marker, lane 2 represents the loading, lane 3 is the flowthrough, from lane 4 to lane 6 are represented the washes (phosphate buffer (50 mM, pH 8.0)), and from lane 7 to lane 10 are represented the elution fractions with sodium citrate buffer (50 mM, pH 3.0)) (B) and (glycine buffer (50 mM, pH 11.0)) (C), respectively.

complete solubilization of polymers and crosslinker, the initiator and catalyst, TEMED (23 µL) and APS (40 µL), were added to promote the crosslinking process (see Figure S3 in Supporting Information). The crosslinking process occurred at 0 °C during 30 min under stirring. 4) Then, casting solutions were frozen at –80 °C for 12 h and lyophilized (Telstar cryodos-50) until dryness (24 h). Magnetic monoliths (see Figure S3, Supporting Information) were prepared following a similar procedure except that after step 2, MNPs (40 mg) were added to each casting solution and the mixture incubated at 80 °C for 24 h in order to promote the polymer adsorption onto MNPs (**Figure 9**). Then the casting solutions followed the same treatment as described in steps (3) and (4).

Preparation of Hybrid Monoliths: Magnetic monoliths were introduced in a plasma chamber which was thoroughly purged with a continuous flow of nitrogen to reduce trace amounts of air and moisture. During the treatment, free radicals were generated under inert-gas discharge environments on selected monoliths surface. Then, 1,6-hexanodiamine was fed to the reaction chamber under vacuum by evaporating the 1,6-hexanodiamine contained in a flask maintained at 150 °C. The plasma treatment occurred at a power setting of 80 W and a constant pressure of 0.3 Torr inside the chamber during 30 min.[48] The extent of amination was determined using the Kaiser test, as in previous works involving the determination of amines in monoliths.[11,40] For immobilization of ligand 4-((4-chloro-6-(3-hydroxyphenoxy)-1,3,5-triazin-2-yl)oxy)naphthalen-1-ol (TPN-BM), an excess of ligand (3 equiv. to the amination content, 150 mg) synthesized according to our previous work,[40] was added to the aminated monolith samples (approximately 60 mg) in DMF (6 mL)

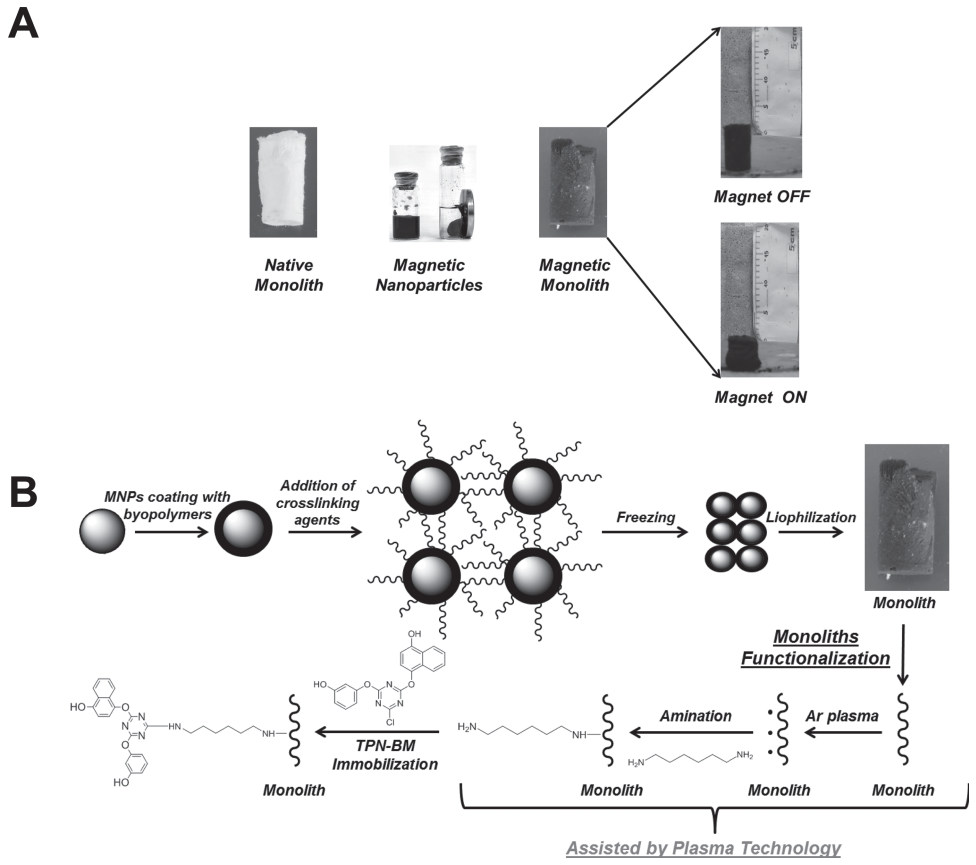

Figure 9. A) Illustration of the materials produced in this work and B) schematic representation of the procedures applied for the production and functionalization of the magnetic monoliths.

and incubated on a rotary shaker (140 rpm) for 72 h at 85 °C. TPN-BM functionalized magnetic monoliths were then washed with DMF until the absorbance at 267 nm, maximum absorbance wavelength of TPN-BM ligand, was ≤ 0.005. In order to assure a complete removal of physically adsorbed ligand, the functionalized monoliths were hosted in a Varian column with 3 mL of capacity and 1 cm of inner diameter, and further washes with DMF and to a cleaning-in-place procedure (CIP) were performed. The CIP procedure involved sequential washing with NaOH (1 M), water (10 mL), regeneration buffer (NaOH 0.1 M in 30% of isopropanol) and again with distilled water (10 mL) until the absorbance at 267 nm was ≤0.005 in each step. The functionalized monoliths were finally washed with sodium phosphate buffer (50 mM, pH 8.0), sodium citrate buffer (50 mM, pH 3.0) and glycine buffer (50 mM, pH 11) until the absorbance at 267 nm was zero. The ligand TPN-BM density was calculated by subtracting the amount of ligand collected in all washes from the initial ligand used in the immobilization step.

Characterization of Native, Magnetic, and Hybrid Monoliths: The morphological and mechanical properties of monoliths before (native) and after MNPs incorporation (magnetic), and after affinity ligand functionalization (hybrid) were investigated using SEM, MIP, water flux measurements and tensile-strain tests. SEM was performed in Hitachi S 2400 equipment with an accelerating voltage set to 15 kV. Firstly, the samples were frozen and broken in liquid nitrogen for cross-sectional analysis and, gold coated before analysis. Monoliths porosity, average pore size diameter and surface area were determined by MIP (Micromeritics, autopore IV). The water fluxes were determined at room temperature and 1 atmosphere. Due to the high porosity of the scaffold network no pressure was applied. Thus, Varian columns (with a capacity of 3 mL and an effective volume of 1.2 mL) were packed with monoliths and charged with distilled water (1 mL). The run time was registered and at least three measurements of distilled water flux were recorded. Uniaxial compression was used to determine the mechanical properties of the monoliths using tensile testing equipment (MINIMAT firmware v.3.1) at room temperature. Samples were prepared in a cylindrical shape (10 mm in diameter thickness). The length between clamps was set at 10 mm, the speed set to 1 mm min^{-1}, a full scale load of 20 N and maximum extension of 90 mm was used. The compression modulus was calculated from the slope of the linear portion of the stress-strain curve.[11] Uniaxial deformation induced by magnetic field was also performed in order to evaluate the response of monoliths at different magnetic fields. Monolithic samples were submitted at different permanent magnetic fields, 0.25, 0.5, 1.5, and 2.5 T, and their deformation, translated by the decrease of monolith's length, was monitored during 20 minutes. At the end, the magnetic field was removed and the reversibility of the magnetic-shape memory was assessed.[56] These tests were performed in dry and wet conditions, since the monoliths magnetic response can change according the hydrate sate of the porous network. X-ray photoelectron spectroscopy (XPS) analyses were performed in order to examine the elemental compositions of native and hybrid monoliths. The studies were conducted on a XSAM800 X-ray spectrometer, operated in the fixed analyser transmission (FAT) mode, with a pass energy of 20 eV, a power of 120 W and using a non-monochromatic radiation from Mg anode ($h\nu = 1253.6$ eV). Spectra were collected with a step of 0.1 eV, using a Sun SPARC Station 4 with Vision software (Kratos). The curve fitting for component peaks was carried out with a non-linear least-squares algorithm using a product of Gaussian and Lorentzian peak shapes. The freeware XPSPeak 4.1 was used. No flood gun was used for charge accumulation neutralization. The charge shift was corrected taking as reference the C 1s binding energy at lower energy equal to 285 eV except in the samples containing the ligand TPN-BM where the value was set

to 284.7 eV due to the existence of sp^2 carbons.[50] Sensitivity factors used were: C 1s – 0.25, O 1s – 0.66, N 1s – 0.44 and Fe $2p_{3/2}$ – 3.0. The stability of hybrid materials was evaluated by immersing them (15 mg) into solutions (500 µL) with different pH values and typical solutions employed in CIP procedures using a 96 well block for 24 hours at 150 rpm. Samples (200 µL) were collected and fresh ones (200 µL) were added in order to maintain the total volume. The ligand leaching was quantified by absorbance at 267 nm and the release of MNP was quantified by the magnetite assay.[57]

Design of a Permanent Magnet: In order to tailor a permanent magnet of 0.5 T with a straight-hole magnet shape to assist chromatographic experiments, FEM studies of a permanent magnet were conducted using Comsol Multiphysics Software to identify the optimal permanent magnet characteristics (magnetic flux density strength in the z-direction, outer diameter and height) for further order. The magnet was designed on purpose and supplied by First4magnets.

Determination of Static and Dynamic Binding Capacities: Partition equilibrium experiments were performed in a batch system as described by Barroso et al,[11,40] in order to estimate the static binding capacities. The adsorption of hIgG and BSA on the native and hybrid monoliths was investigated. Monolith samples (10 mg) were incubated with hIgG and BSA (0.0–60 mg mL^{-1}, 500 µL) prepared in phosphate buffer (50 mM, pH 8.0). All experiments were performed in duplicates at 25 °C, at a stirring rate of 200 rpm for 24 h. After incubation, the amount of protein in the supernatants was quantified at 280 nm on a microplate reader (Tecan Infinite F200, filter, $\lambda = 280$ nm). In the meanwhile, a calibration curve was prepared using hIgG and BSA in phosphate buffer solutions (50 mM, pH 8.0) (0.0–60 mg mL^{-1}). The adsorption phenomena followed the Langmuir–Freundlich model represented by:

$$q = \frac{Q_m \times (C)^n}{K_d + (C)^n} \quad (1)$$

where K_d is the apparent dissociation constant (M) that includes contributions from ligand binding to support, Q_m is the maximum binding capacity (mg protein g^{-1} support), C is the concentration of protein in the liquid at the equilibrium (M) and n represents the Langmuir–Freundlich coefficient. The dynamic loading capacity of the packed columns with magnetic and hybrid magnetic monoliths, was determined using frontal analysis according to:

$$Q = \frac{V_e}{[\text{Protein}]_{\text{plateau}}} \quad (2)$$

where Q corresponds to the estimated adsorbent capacity and V_e corresponds to the elution volume. This procedure consisted in loading hIgG and BSA solutions (6 mL, 0.5 mg mL^{-1}) in sodium phosphate buffer (50 mM, pH 8.0) through the equilibrated monolithic packed columns at approximately 1 mL min^{-1} until the protein concentration of the output and input streams were equal. At that point, packed monolithic columns were washed with phosphate buffer (50 mM, pH 8.0) to remove unbound protein and the bound protein was eluted using two different buffers, sodium citrate buffer (50 mM, pH 3.0) and glycine buffer (50 mM, pH 11.0). Samples collected (1 mL) during loading, washing and elution stages were examined by measuring absorbance at 280 nm on a 96-well format.

Capture and Release of IgG from Pure Solutions: The affinity capturing experiments were performed in a step wise adsorption–desorption process by switching eluents at room temperature and at atmospheric pressure. Columns (with diameter and length 1 and 7 cm, respectively) were packed with hybrid monoliths, and then washed and equilibrated as described in previous section. Then, hIgG (1 mL) and BSA solution (3 mg mL^{-1}) were added and columns were washed with sodium phosphate buffer (50 mM, pH 8.0) until the absorbance measured at 280 nm reached ≤0.005. The bound protein was recovered with two elution buffers, either sodium citrate buffer (50 mM, pH 3.0) or glycine buffer (50mM, pH 11.0) with and without magnetic compression. Packed columns with functionalized magnetic monoliths were then regenerated as previously described (CIP step). These chromatographic experiments were repeated during 3 cycles and one more after auto-claving (sterilization in place, SIP) in order to estimate the column capacity over time. The total amount of protein bound, eluted and regenerated from the affinity magnetic monoliths was initially determined by absorbance measured at 280 nm and by the BCA method (microplate reader assay).[11]

Purification of Monoclonal Antibodies from Cell Supernatants: In order to evaluate the possibility to capture monoclonal antibodies (mAbs) directly from non-clarified crude extracts, columns packed with hybrid CP monoliths were tested with a mammalian crude extract solution (1 mL, 2 mg of total protein per millilitre). After crude extract loading, packed columns were washed with sodium phosphate buffer (5 mL, 50 mM, pH 8.0) until the absorbance measured at 280 nm reached ≤0.005, and the bound protein was further eluted with sodium citrate buffer (50 mM, pH 3.0) or glycine buffer (50 mM, pH 11) in the presence of magnetic field. All collected samples were analysed by the BCA assay to quantify the amount of total protein bound and eluted from the monoliths. SDS-PAGE was performed on acrylamide gel (12.5%) in Tris-Glycine buffer system pH 8.3. Electrophoresis apparatus (from BIO-RAD) was connected with power supply at 120 V, 190 mA for 1 h. The gel was revealed using a silver staining kit from BIO-RAD.

Acknowledgements

The authors would like to thank the financial support from Fundação para a Ciência e Tecnologia, Portugal, through contracts PEst-C/EQB/LA0006/2011, MIT-Pt/BS-CTRM/0051/2008, PTDC/EBB-BIO/102163/2008, PTDC/EBB-BIO/098961/2008 and PTDC/EBB-BIO/118317/2010 and doctoral grant SFRH/BD/62475/2009 (T.B.), Fundação Calouste Gulbenkian, FEDER and FSE. The authors acknowledge the Analytical Services Laboratory of REQUIMTE for the characterization of materials. Authors are also thankful to Lonza Biologics, UK (Dr. Richard Alldread) and the Animal Cell Technology Unit of ITQB-UNL/IBET (Dr. Paula M. Alves and Dr. Ana Teixeira) for providing the cell culture bulks of antibodies.

Received: January 4, 2014
Revised: February 13, 2014
Published online: April 14, 2014

[1] B. V. Ayyar, S. Arora, C. Murphy, R. O'Kennedy, *Methods* **2012**, *56*, 116.
[2] A. Azevedo, M. Aires-Barros, *Hybridoma* **1999**, *18*, 297–303.
[3] P. A. Marichal-Gallardo, M. M. Alvarez, *Biotechnol. Progr.* **2012**, *28*, 899.
[4] L. Rowe, G. El Khoury, C. R. Lowe, *Affinity chromatography: historical and prospective overview*, (Ed: G. Subramanian), Wiley-VCG Verlag GmbH & Co. KGaA, Weinheim, Germany **2012,** pp. 225–282.
[5] A. Jungbauer, R. Hahn, *J. Sep. Sci.* **2004**, *27*, 767.
[6] A. Namera, A. Nakamoto, T. Saito, S. Miyazaki, *J. Sep. Sci.* **2011**, *34*, 901.
[7] J. Sproß, A. Sinz, *J. Sep. Sci.* **2011**, *34*, 1958.
[8] R. D. Arrua, C. I. Alvarez Igarzabal, *J. Sep. Sci.* **2011**, *34*, 1974.
[9] E. Calleri, S. Ambrosini, C. Temporini, G. Massolini, *J. Pharm. Biomed. Anal.* **2012**, *69*, 64.
[10] E. Lansing, *J. Macromol. Sci. Polym. Rev.* **2007**, *3*, 481.
[11] T. Barroso, A. C. A. Roque, A. Aguiar-Ricardo, *RSC Adv.* **2012**, *2*, 11285.
[12] S. Sun, Y. Tang, Q. Fu, X. Liu, W. Du, L. Guo, Y. Zhao, *J. Sep. Sci.* **2012**, *35*, 1.
[13] R. Mallik, D. S. Hage, *J. Sep. Sci.* **2006**, *29*, 1686.
[14] P. E. Gustavsson, P. O. Larsson, *J. Chromatogr. A* **2001**, *925*, 69.
[15] S. G. Lévesque, R. M. Lim, M. S. Shoichet, *Biomaterials* **2005**, *26*, 7436.

[16] J. M. Dang, K. W. Leong, *Adv. Drug Delivery Rev.* **2006**, *58*, 487.
[17] A. M. G. C. Dias, A. Hussain, A. S. Marcos, A. C. A. Roque, *Biotechnol. Adv.* **2011**, *29*, 142.
[18] S.-W. Choi, J. Xie, Y. Xia, *Adv. Mater.* **2009**, *21*, 2997.
[19] S. Boddohi, M. J. Kipper, *Adv. Mater.* **2010**, *22*, 2998.
[20] N. Bhattarai, Z. Li, J. Gunn, M. Leung, A. Cooper, D. Edmondson, O. Veiseh, M.-H. Chen, Y. Zhang, R. G. Ellenbogen, M. Zhang, *Adv. Mater.* **2009**, *21*, 2792.
[21] A. Kumar, A. Srivastava, I. Y. Galaev, B. Mattiasson, *Prog. Polym. Sci.* **2007**, *32*, 1205.
[22] D. Ratna, J. Karger-Kocsis, *J. Mater. Sci.* **2007**, *43*, 254.
[23] X. Zhao, J. Kim, C. a Cezar, N. Huebsch, K. Lee, K. Bouhadir, D. J. Mooney, *Proc. Natl. Acad. Sci. U.S.A.* **2011**, *108*, 67.
[24] D. Le Sage, K. Arai, D. R. Glenn, S. J. DeVience, L. M. Pham, L. Rahn-Lee, M. D. Lukin, a. Yacoby, a. Komeili, R. L. Walsworth, *Nature* **2013**, *496*, 486.
[25] P. W. Goodwill, E. U. Saritas, L. R. Croft, T. N. Kim, K. M. Krishnan, D. V. Schaffer, S. M. Conolly, *Adv. Mater.* **2012**, *24*, 3870.
[26] R. Hao, R. Xing, Z. Xu, Y. Hou, S. Gao, S. Sun, *Adv. Mater.* **2010**, *22*, 2729.
[27] B. Chertok, B. a Moffat, A. E. David, F. Yu, C. Bergemann, B. D. Ross, V. C. Yang, *Biomaterials* **2008**, *29*, 487.
[28] I. Koh, X. Wang, B. Varughese, L. Isaacs, S. H. Ehrman, D. S. English, *J. Phys. Chem. B* **2006**, *110*, 1553.
[29] I. L. Batalha, A. Hussain, A. C. A. Roque, *J. Mol. Recognit.* **2010**, *23*, 462.
[30] M. Franzreb, M. Siemann-Herzberg, T. J. Hobley, O. R. T. Thomas, *Appl. Microbiol. Biot.* **2006**, *70*, 505.
[31] T. Griffin, K. Mosbach, R. Mosbach, *Appl. Biochem. Biotechnol.* **1981**, *6*, 283.
[32] N. R. Nagireddy, M. M. Yallapu, V. Kokkarachedu, R. Sakey, V. Kanikireddy, J. Pattayil Alias, M. R. Konduru, *J. Polym. Res.* **2011**, *18*, 2285.
[33] Y.-Y. Liang, L.-M. Zhang, W. Jiang, W. Li, *ChemPhysChem* **2007**, *8*, 2367.
[34] A. Kumar, A. Srivastava, *Nat. Protoc.* **2010**, *5*, 1737.
[35] M. Temtem, T. Barroso, T. Casimiro, J. F. Mano, A. Aguiar-Ricardo, *J. Supercrit. Fluid* **2012**, *66*, 398.
[36] M. Furlan, B. Brand, M. Lattuada, *Soft Matter* **2010**, *6*, 5636.
[37] F. Plieva, A. Oknianska, E. Degerman, I. Y. Galaev, B. Mattiasson, *J. Biomater. Sci.* **2006**, *17*, 1075.
[38] T. Desmet, R. Morent, N. De Geyter, C. Leys, E. Schacht, P. Dubruel, *Biomacromolecules* **2009**, *10*, 2351.
[39] R. Morent, N. De Geyter, *Plasma Process. Polym.* **2011**, *8*, 171.
[40] T. Barroso, A. Lourenço, M. Araújo, V. Bonifácio, A. C. A. Roque, A. Aguiar-Ricardo, *J. Mol. Recognit.* **2014**, 28, 25.
[41] M. Wang, J. Xu, X. Zhou, T. Tan, *Biochem. Eng. J.* **2007**, *34*, 76.
[42] V. G. Correia, M. Coelho, T. Barroso, V. P. Raje, D. B. Vasco, T. Casimiro, M. G. Pinho, A. Aguiar-Ricardo, *Biofouling* **2013**, *29*, 273.
[43] S. Nandi, B. Kundu, D. Basu, *Mater. Sci. Eng. C* **2013**, *33*, 1.
[44] A. I. Cooper, A. B. Holmes, *Adv. Mater.* **1999**, *11*, 1270.
[45] J. Wang, M. Hon, *J. Biomed. Mater. Res.* **2002**, *64A*, 262.
[46] C.-F. Dai, C.-J. Weng, P.-R. Li, J.-M. Yeh, *Polym. Degrad. Stabil.* **2010**, *95*, 600.
[47] S. Manolache, F. Denes, *Polym. Bull.* **2001**, *47*, 329.
[48] O. Kolluri, R. Johanson, Plasma deposited film networks, *US Patent 5,723,219* **1998**, 1–13.
[49] T. Barroso, M. Temtem, A. Hussain, A. Aguiar-Ricardo, A. C. A. Roque, *J. Memb. Sci.* **2010**, *348*, 224.
[50] G. Beamson, D. Briggs, *High resolution XPS of organic polymers: the Scienta ESCA300 database* **1992**.
[51] T.-C. Lin, G. Seshadri, J. A. Kelber, *Appl. Surf. Sci.* **1997**, *119*, 83.
[52] A. V. Naumkin, A. Kraut-Vass, S. W. Gaarenstroom, C. J. Powell, *NIST X-ray Photoelectron. Spectrosc. Database* **2012**.
[53] R. Wongchuphan, B. T. Tey, W. S. Tan, F. S. Taip, S. M. M. Kamal, T. C. Ling, *Biochem. Eng. J.* **2009**, *45*, 232.
[54] R. J. Umpleby, S. C. Baxter, Y. Chen, R. N. Shah, K. D. Shimizu, *Anal. Chem.* **2001**, *73*, 4584.
[55] A. Leyva, A. Quintana, M. Sánchez, E. N. Rodríguez, J. Cremata, J. C. Sánchez, *Biologicals* **2008**, *36*, 134.
[56] P. Müllner, V. A. Chernenko, G. Kostorz, *J. Magn. Magn. Mater* **2003**, *267*, 325.
[57] R. Sabaté, R. Barnadas-Rodríguez, J. Callejas-Fernández, R. Hidalgo-Alvarez, J. Estelrich, *Int. J. Pharm.* **2008**, *347*, 156.
[58] T. Barroso, A. Hussain, A. C. A. Roque, A. Aguiar-Ricardo, *Biotechnol. J.* **2013**, *8*, 1.